ENERGY ABSORPTION CAPACITY OF STEEL BEAMS SUBJECTED TO CYCLIC BENDING MOMENT

K. Haneda [1], S. Yamazaki [2] and S. Minami [3]

[1] *M. Eng., Structural Engineering Div., Nihon Sekkei, Inc., Tokyo, Japan*
[2] *Prof. Emeritus, Tokyo Metropolitan University, Tokyo, Japan*
[3] *Assistant Prof., Dept. of Architecture and Building Engineering, Tokyo Metropolitan University, Tokyo, Japan*
Email: haneda-k@nihonsekkei.co.jp, minami-susumu@c.metro-u.ac.jp

ABSTRACT:

When buildings are subjected to long-period ground motions, the number of cycles of overloading can be of several orders, leading to the formation of plastic zones. The energy absorption capacity of the beams of buildings is an important parameter to be considered during the evaluation of the seismic capacity of frames with weak beams. In this study, we quantitatively evaluate the relation between the number of loading cycles and the energy absorption capacity of beams by performing a series of experiments on specimens with an identical shape subjected to cyclic loading. The experimental results show the relation between the energy absorption capacity of beams under monotonic loading (η_0) and cyclic loading (η_d), the average of the half-cycle energy ($\Delta\eta_m$), and the number of effective half-cycles (N_e). Moreover, a method for estimating η_0 is also proposed.

KEYWORDS: Experiment, Cyclic loading, Energy absorption capacity, Number of half-cycles, Energy absorption capacity under monotonic loading, Mean of half-cycle energy

1. INTRODUCTION

In recent years, long-period ground motions generated by huge offshore earthquakes have been studied intensively. These studies have revealed that when buildings are subjected to long-period ground motions, the number of cycles of loading can be of several orders, leading to the formation of plastic zones in the beams of buildings. The energy absorption capacity of beams is an important parameter to be considered in the evaluation of the seismic capacity of frames with weak beams. However, previous studies on the energy absorption capacity of beams have mostly focused on the details of connections or joint shapes. There have been few studies on the influence of the cyclic loading history on the energy absorption capacity of beams. In addition, very few researches have examined the influence of the number of cycles of loading on the beams.
In this study, the influence of the cyclic loading history on the energy absorption capacity of H-shaped steel beam specimens is experimentally investigated. In addition, the relation between the number of loading cycles and the energy absorption capacity is quantitatively evaluated from cyclic loading experiments using beam specimens having identical shapes for different amplitudes and loading patterns.

2. EXPERIMENTAL METHOD

2.1. Specimens

In this experiment, cantilever-type specimens as shown in Figure 1, are used. These specimens have six different types of cross sections, and the lengths of all the specimens are 1 m. The specimens are H-shaped welded built-up steel beams, and the web connections at the end of the beams are either welded joints (W) or high-tension-bolted joints (B). Some specimens have stiffeners to prevent local buckling. The shapes of the specimens and the details of their joints are also shown in Figure 1. The names and the shapes of all the specimens are listed in Table 1.
The specimens have been named on the basis of their cross-sectional shapes, the type of web connection, the presence of stiffeners, and the loading history, as shown below.

	Beam Cross Section	Web Joint Type	Presence of Stiffener	Type of Loading History		Specimen Name
(Sample 1)	G1	B (HTB)	R (Yes)	I2	=	G1BR-I2
(Sample 2)	G4	W (weld)	N (No)	RW	=	G4WN-RW

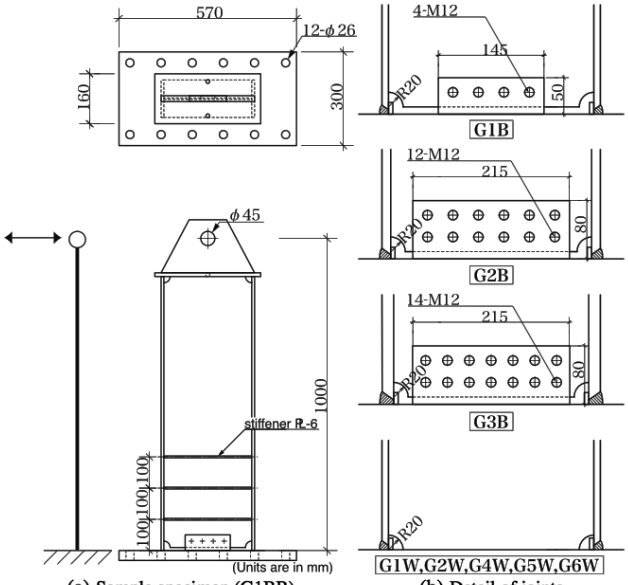

(a) Sample specimen (G1BR) (b) Detail of joints

Figure 1 Shapes of specimens

Table 2 Earthquake waves for randam loading

Abbreviation	Wave Name	Wave	Duration Time
RE	EL CENTRO NS	Observed	24.4 s
RW	KK-WOS-EW[1)]	Simulated	179.4 s
RS	C-SAN-EW[1)]	Simulated	120.0 s

Note: 1) See Reference [AIJ].

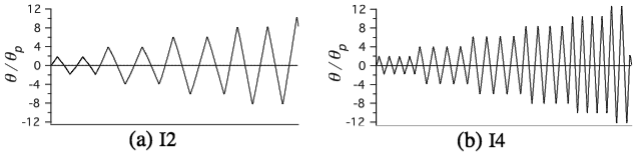

(a) I2 (b) I4

Figure 2 Cyclic loading histories of incremental amplitude procedure

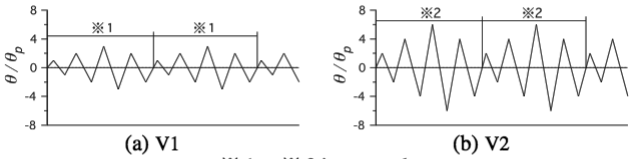

(a) V1 (b) V2

※ 1 or ※ 2 is repeated.

Figure 3 Cyclic loading histories of patterned amplitude procedure

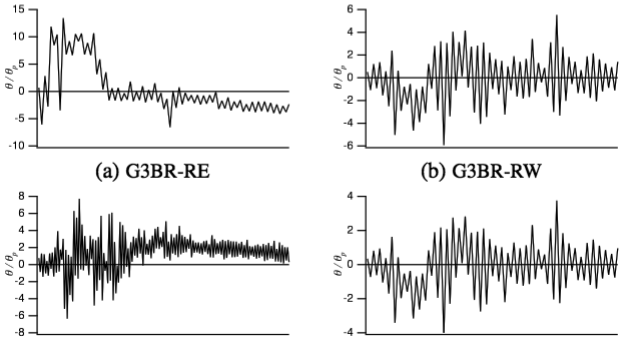

(a) G3BR-RE (b) G3BR-RW

(c) G3BR-RS (d) G4BR-RW

Figure 4 Random loading history

2.2. Loading Procedure

The end plate on the fixed side of the specimens is set as a supporting jig using high-tension bolts, and the free-end side is connected to the pin joints. The specimens are subjected to static loading by displacement control of the loading point at the pin joint. The out-of-plate displacement at the loading point is restricted.

2.3. Loading History

The following are the four types of loading histories employed in this experiment.

a. Monotonic loading history

One-way loading is performed until the specimen loses its resistance to moment. This type of loading history is indicated by MO.

b. Cyclic loading history obtained using an incremental amplitude procedure

In this type of loading history, the amplitude increases with the number of loading cycles. The amplitude depends on the full plastic deformation (θ_p), which is the angle formed when the beam-end moment M attains a full plastic moment M_p. The increment in the amplitude is set as $2\theta_p$. The cyclic loading histories, I2 and I4, are illustrated in Figure 2.

c. Cyclic loading history obtained using a patterned amplitude procedure

The cyclic loading histories of V1 and V2 are illustrated in Figure 3. The patterned part of ※1 or ※2, as shown in this figure, is repeated until the failure of the specimen. The increment in the amplitude is set as θ_p and $2\theta_p$ for V1 and V2, respectively.

d. Random loading history

Random loading history is based on the result of an earthquake response analysis of frames with weak beams. Table 2 lists the abbreviations used for each type of loading history, the natural period of the frame model used in the analysis, and the earthquake waves. The different types of random loading histories used in the experiments are shown in Figure 4. The loading history is repeated until the failure of the specimen.

Table 1 Experimental results for each Specimen

Specimen Name	Section	Web Joint	Presence of Stiffener	M_p [kN·m]	θ_p [rad]	Failure Mode	α	N_e	η_d	$\Delta\eta_m$
G1BR-I2	H–300×120×4.5×9	HTB	Yes	167.6	6.38×10^{-3}	F1	1.05	6	10.5	2.31
G1BR-I4						F1	1.02	10	14.3	1.90
G1WN-I2		Weld	No			L1	1.15	10	36.8	4.88
G1WN-I4							1.13	15	40.2	3.55
G2BR-I2	H–300×120×6×12	HTB	Yes	227.6	6.59×10^{-3}	F1	1.22	11	39.9	4.75
G2BR-I4						F1	1.19	18	47.8	3.48
G2BR-MO						F1	1.30	1	11.2	14.7
G2BR-V2						F1	1.25	14	49.8	4.66
G2WN-I2		Weld	No			L2	1.27	16	134.5	11.0
G2WN-I4							1.24	27	147.8	7.17
G2WN-V2							1.24	44	161.5	4.81
G2WR-I2			Yes			F1	1.32	13	68.7	6.92
G2WR-I4						F2	1.40	27	162.9	7.90
G3BR-MO	H–300×120×6×16	HTB	Yes	276.9	7.03×10^{-3}	F1	1.31	1	13.4	18.5
G3BR-I2						F2	1.31	16	97.4	8.37
G3BR-V1						F2	1.15	87	129.9	2.06
G3BR-RW						F2	1.23	82	154.7	2.60
G3BR-RE						F1	1.28	4	25.5	8.79
G3BR-RS						F1	1.24	18	46.3	3.54
G4WN-MO	H–300×120×4.5×12	Weld	No	176.6	5.94×10^{-3}	L1	1.14	1	10.3	14.4
G4WN-I2							1.20	10	39.3	5.51
G4WN-I4							1.18	13	34.3	3.69
G4WN-V1							1.19	42	65.1	2.17
G4WN-RW							1.20	60	62.3	1.45
G5WN-MO	H–350×120×4.5×9	Weld	No	187.9	5.41×10^{-3}	L1	1.09	1	7.46	10.5
G5WN-I2							1.13	9	30.1	4.68
G5WN-I4							1.14	15	41.2	3.85
G6WN-MO	H–250×120×4.5×9	Weld	No	125.8	6.93×10^{-3}	L1	1.23	1	16.5	20.8
G6WN-I2							1.22	12	57.5	6.04
G6WN-I4							1.24	19	75.5	5.01

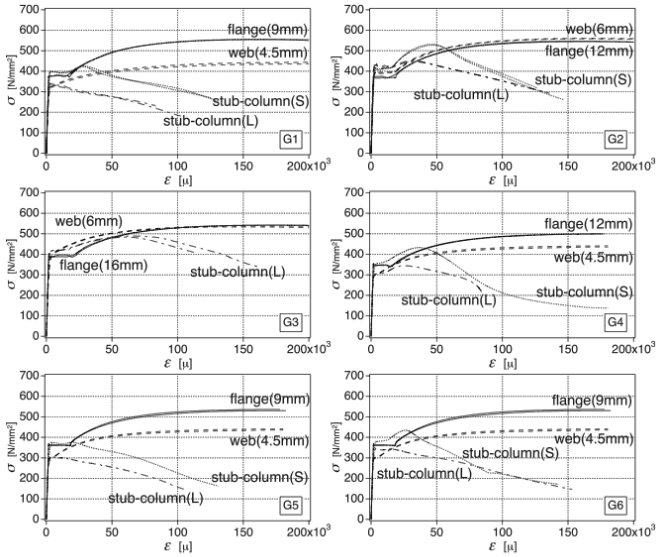

Figure 5 Results of coupon test and stub–column test

Table 3 Mechanical properties of steel

Section	Sample	σ_y	σ_B	Section	Sample	σ_y	σ_B
G1	Web	321	440	G4	Web	300	439
	Flange	376	555		Flange	346	500
	L	340	—		L	303	344
	S	398*	425		S	354*	433
G2	Web	394	559	G5	Web	300	439
	Flange	373	545		Flange	361	533
	L	439	449		L	306	—
	S	412*	530		S	371*	376
G3	Web	392	536	G6	Web	300	439
	Flange	391	542		Flange	361	533
	L	420*	486		L	347	—
		[N/mm^2]			S	380*	434

Table 4 Failure mode

Cause of deteriorating	Situation at failure	Abbreviation
Local buckling	Loss of bearing force without flange fracture	L1
	Loss of bearing force by flange fracture	L2
Flange fracture	Crack growth from center of weld joint of flange	F1
	Crack growth from edge of weld joint of flange	F2

3. EXPERIMENTAL RESULTS

3.1. Characteristics of Steel

The results of a coupon test and stub-column test on steel are shown in Figure 5. Stub-column specimens can be of two types, depending on their cross sections—those having the same cross section as the beam specimen, termed as L, and those having a cross section that is half the depth of the beam specimen, termed as S. The heights of all the stub-column specimens are three times the width of the beam specimen.

3.2. Load–Displacement Relation

The loading history and load–displacement relation for each cyclic loading experiment is shown in Figure 6. The load–displacement relation is normalized by M_p and θ_p. The values of M_p and θ_p are listed in Table 1. The values of M_p are calculated using σ_y, which is obtained from the stub-column test. The values used in the calculation are listed in Table 3 and indicated by the * sign.

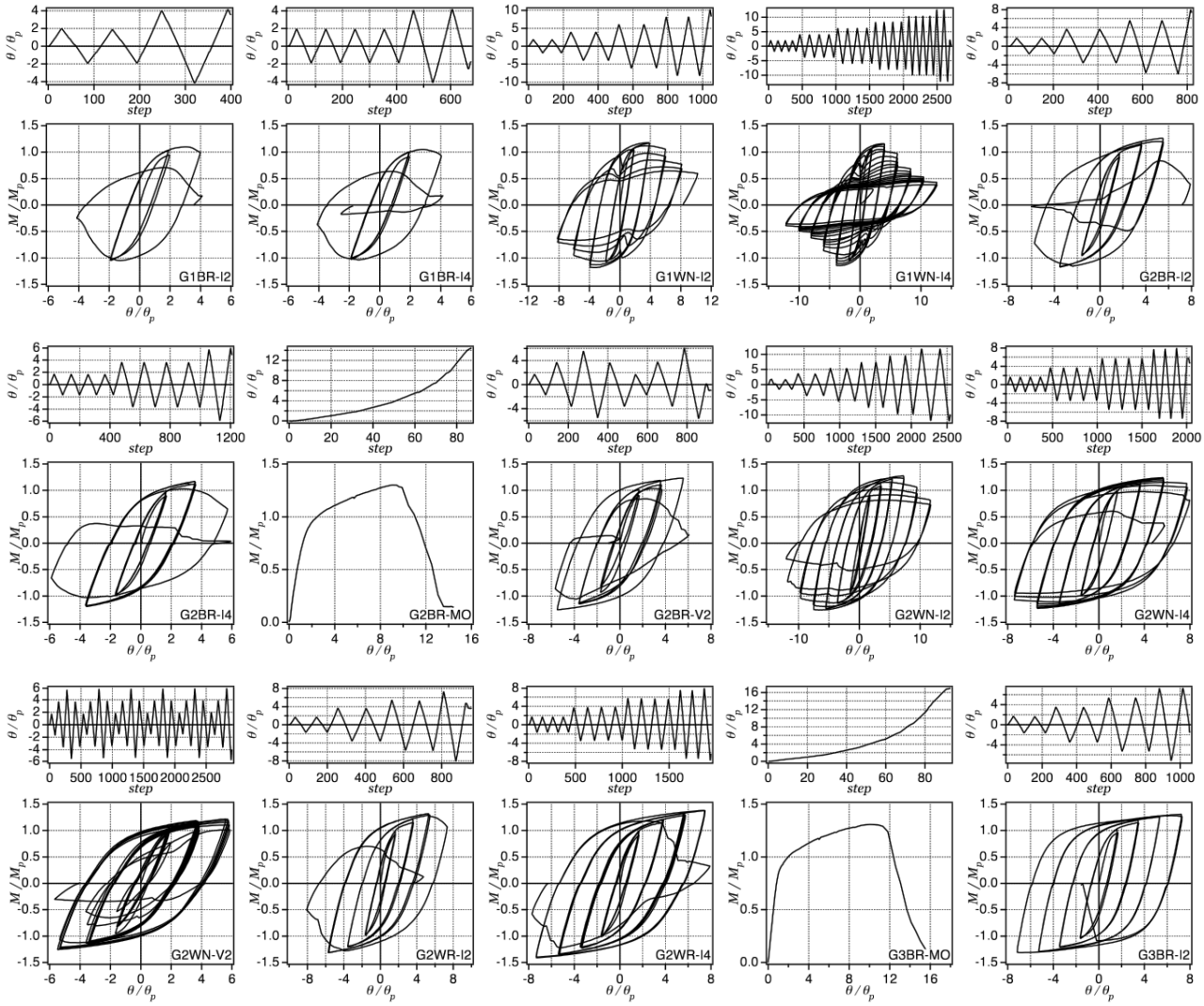

Figure 6 Loading history and load–displacement relation (Part 1)

3.3. Failure Modes

The failure characteristics of each specimen are classified into four types of failure modes, as listed in Table 4, and the failure modes of the specimens are listed in Table 1. In this paper, the specimens exhibiting the L1 or L2 failure modes are referred to as local-buckling-type specimens, and those exhibiting the F1 or F2 failure modes are referred to as flange-fracture-type specimens. For specimens G2WR and G3BR, different failure modes, i.e., the F1 and F2 failure modes, are observed even though they have the same shape.

3.4. Half-cycle Energy and Number of Effective Half-cycles

In this study, the point when the beam end moment finally attains the full plastic moment M_p is assumed to be the upper limit of the energy absorption capacity (See Figure 7). As shown in Figure 8, a half-cycle is completed when the value of M starts from zero, reaches M_p, and then reaches zero again. Effective half-cycles are those half-cycles whose energies exceed 5% of the maximum half-cycle energy absorption amount. The number of effective half-cycles up to the limit point is counted, and this number is called as the "number of effective half-cycles (N_e)." Figure 9 shows an example of the energy absorption amount for different half-cycles. The shaded bars in this figure correspond to the effective half-cycles, and they extend up to the limit point.

3.5. Definition of Cumulative Plastic Deformation Ratio

The cumulative plastic deformation ratio (η_d) is defined using the energy absorption capacity.

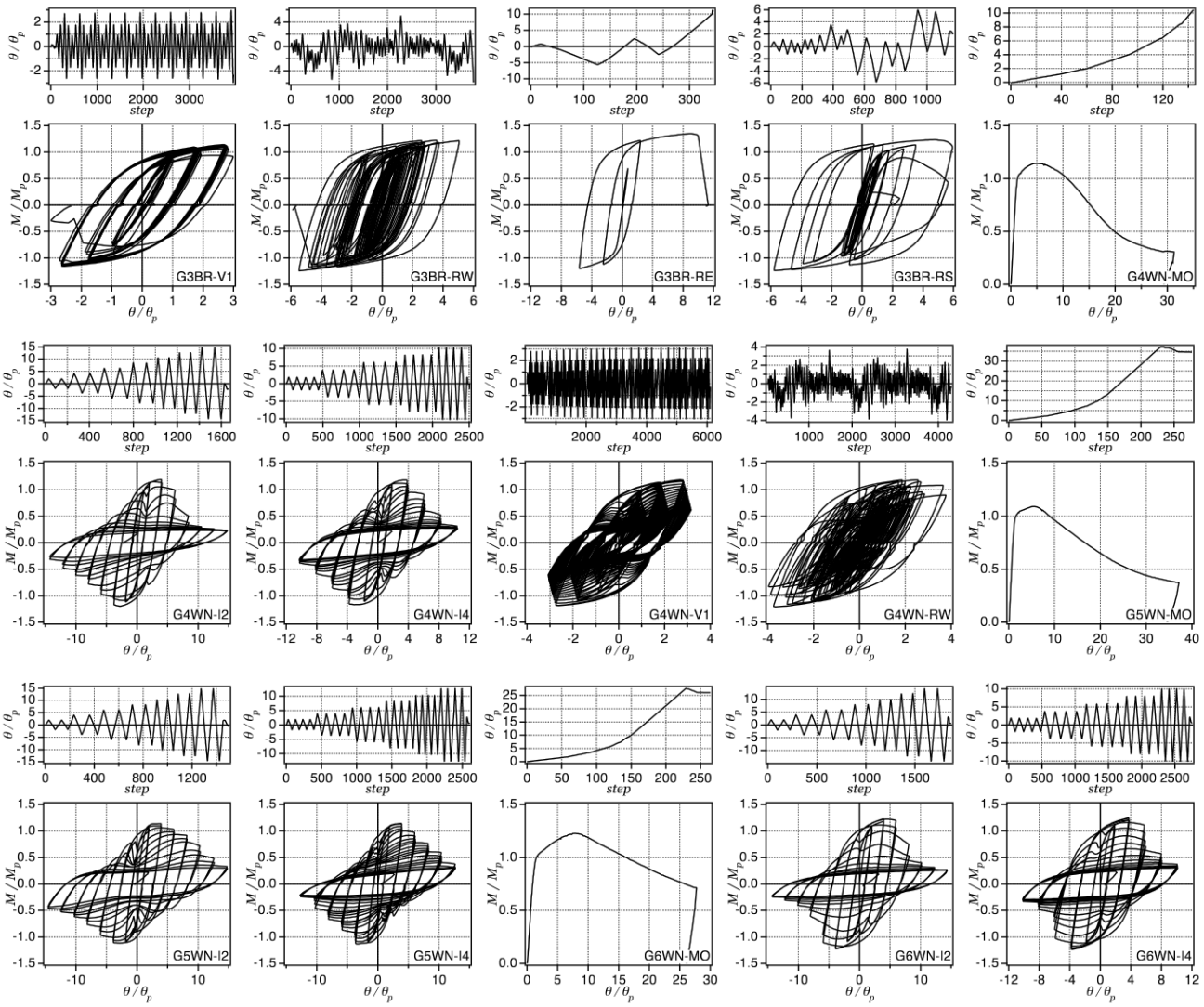

Figure 6 Loading history and load–displacement relation (Part 2)

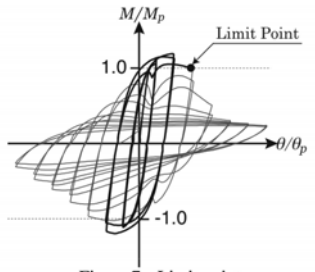

Figure 7 Limit point

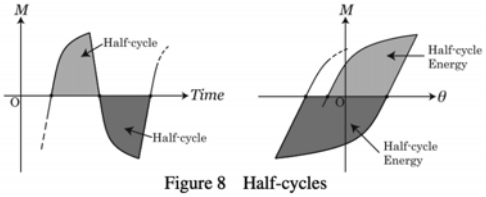

Figure 8 Half-cycles

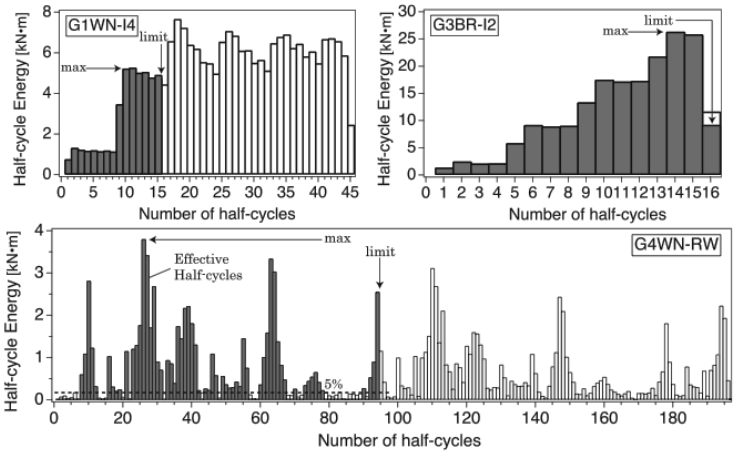

Figure 9 Example of effective half-cycles

$$\eta_d = \frac{W_d}{M_p \cdot \theta_p} \tag{1}$$

Here, W_d is the sum of the effective half-cycle energy.

The η_d values for each specimen are listed in Table 1. The η_d value for a specimen subjected to monotonic loading is indicated by η_0, and that for specimens with different cross sections and different types of joints can be

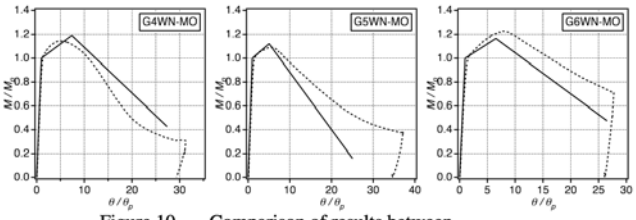

Figure 10 Comparison of results between monotonic loading prediction equation[2)]
(Note: 2) See Reference [Kato].)

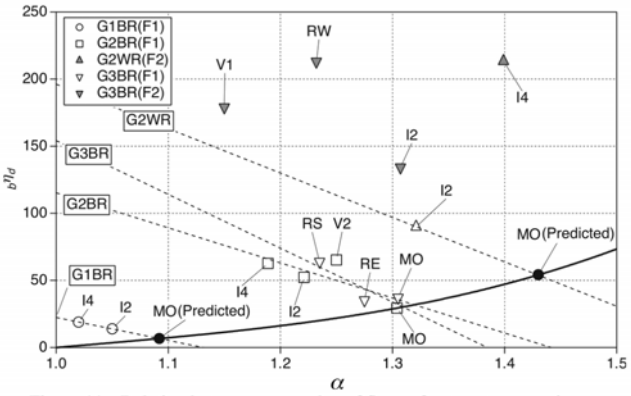

Figure 11 Relation between ${}_b\eta_d$ and α of flange-fracture-type specimens

compared by standardizing η_d by dividing it by η_0. The value of η_0 for a specimen that has not been subjected to monotonic loading is predicted using the method described in the following section.
For specimens under monotonic loading, it is assumed that the energy absorption capacities for positive and negative bendings are equal. The cumulative plastic deformation ratio is doubled ($2\eta_0$), and N_e is assumed to be equal to 2 for the comparison of the energy absorption capacities of the specimens under cyclic and monotonic loadings.

4. DETERMINATION OF ENERGY ABSORPTION CAPACITY OF SPECIMEN UNDER MONOTONIC LOADING

4.1. Local-buckling-type Specimens

Kato et al. have approximated the load–displacement relation using three parts that exhibit linear relations—the elastic part, the strain-hardening part, and the deteriorating part—by a post-buckling analysis [Kato]. Figure 10 shows the comparison between the results of the monotonic loading experiments and the results obtained using a prediction equation [Kato]. The dotted line indicates the experimental results, and the solid line indicates the results obtained from the prediction equation. Both the results are found to correspond roughly. It is assumed that η_0 can also be determined by using the prediction equation. The value of η_0 for specimens G1WN and G2WN can be determined using the prediction equation.

4.2. Flange-fracture-type Specimens

The energy absorption capacity of a flange-fracture-type specimen under monotonic loading is estimated by determining the relation between the maximum strength ratio α and the energy absorption capacity. α is calculated as follows:

$$\alpha = \frac{M_{\max}}{M_p} \tag{2}$$

where $M_{\max}$: maximum moment of the end of the beam and
M_p : full plastic moment of the beam.

The cumulative plastic deformation ratio ${}_b\eta_d$ of flange-fracture-type specimens is given as follows:

$${}_b\eta_d = \frac{W_d}{M_p \cdot \theta_{pb}} \tag{3}$$

where θ_{pb} : bending component in θ_p.
In addition, the relation between ${}_b\eta_d$ and η_d is obtained by the following equation.

$${}_b\eta_d = \eta_d(1+\frac{k_b}{k_s}) \tag{4}$$

where k_b : bending stiffness of a beam and
k_s : shear stiffness of the beam.

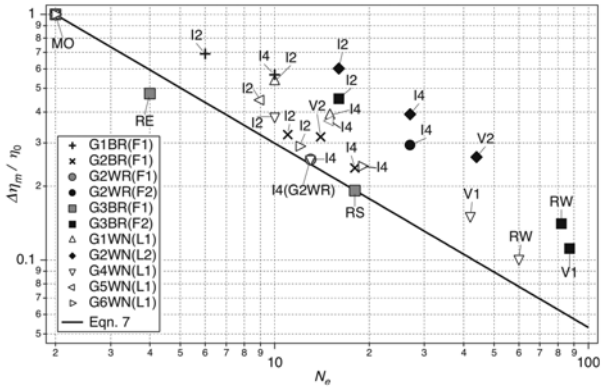

Figure 12 Relation between $\Delta\eta_m$ and N_e

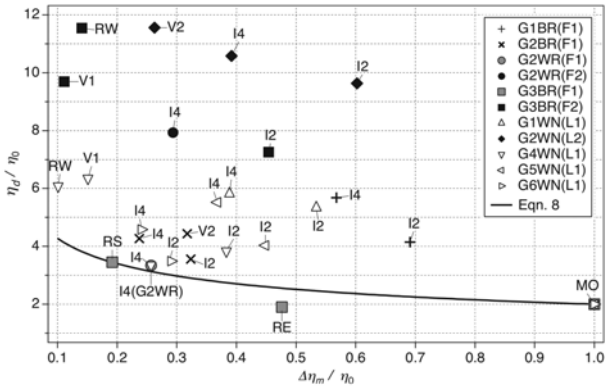

Figure 13 Relation between η_d and $\Delta\eta_m$

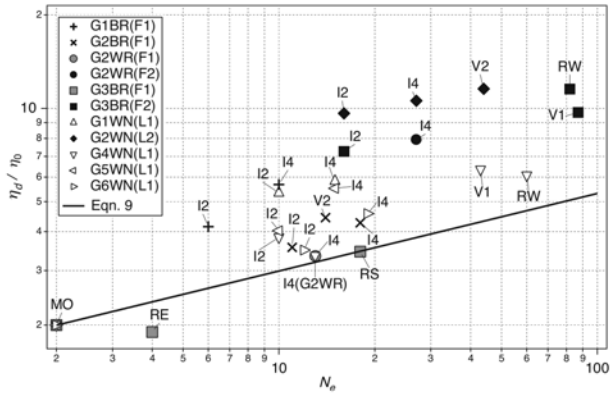

Figure 14 Relation between η_d and N_e

${}_b\eta_d$ is defined as the cumulative plastic deformation ratio of flange-fracture-type specimens when the shear deformation is maintained within the elastic range. If ${}_b\eta_d$ is used, the energy absorption capacity of the beam under monotonic loading is unaffected by its cross section, shape, and length. Therefore, the energy absorption capacity can be expressed only as a function of the maximum strength ratio. In the case of monotonic loading, α is indicated by α_0, and ${}_b\eta_d$ is indicated by ${}_b\eta_0$. The monotonic loading analysis, which is based on the stress–strain relation that corresponds to an average steel material characteristic of the 490 N/mm^2 class, yields the following expression: $\alpha_0 - 2_b\eta_0$. Further, the following expression has been derived:

$$ {}_b\eta = 2(-225.4 + 590.6\alpha - 541.1\alpha^2 + 175.9\alpha^3) \tag{5}$$

The relation between α and ${}_b\eta_d$ is shown in Figure 11, where the results (α, $2_b\eta_0$) of the monotonic loading experiments and Eqn. 5 are also shown. These plots correspond to the G2BR-MO and G3BR-MO plots. It can be observed that (α, ${}_b\eta_d$) obtained from the cyclic loading experiments and (α, $2_b\eta_0$) obtained from the monotonic loading experiments exhibit an almost linear relation. Thus, there exists a linear relation between the results of Eqn. 5 and ${}_b\eta_0$ of the test specimens that have not been subjected to monotonic loading. Figure 11 shows the straight lines corresponding to the F1 failure mode, where ${}_b\eta_d$ obtained from the tests is a straight regression line. The slope of the straight regression line of specimen G2WR corresponds to the average slope of the lines of specimens G2BR and G3BR, and the straight regression line intersects the straight line of specimen G2WR-I2. The estimated values of $2_b\eta_0$ of the specimens that have not been subjected to monotonic loading, indicated by "●," are assumed to be the intersection of the straight regression lines and Eqn. 5.

5. ENERGY ABSORPTION CAPACITY OF SPECIMENS UNDER CYCLIC LOADING

The energy absorption capacity of specimens under cyclic loading is obtained using η_d, η_0, N_e, and the mean of half-cycle energy, $\Delta\eta_m$. $\Delta\eta_m$ is obtained by dividing η_d by N_e, as shown in the following equation:

$$\Delta\eta_m = \frac{\eta_d}{N_e} \tag{6}$$

Figure 12 shows the relation between ($\Delta\eta_m / \eta_0$) and N_e on a log–log scale. All test parameters exhibit an almost linear relation. The curve in this figure corresponds to the lower-limit line of the $\Delta\eta_m / \eta_0 - N_e$ relation, and the following equation provides the following expression for this lower-limit line.

$$\frac{\Delta\eta_m}{\eta_0} = 1.68 N_e^{-0.75} \tag{7}$$

By substituting Eqn. 6 in Eqn. 7 and eliminating N_e, it is possible to obtain the relation between η_d / η_0 and $\Delta\eta_m / \eta_0$.

$$\frac{\eta_d}{\eta_0} = 2.0\left(\frac{\Delta\eta_m}{\eta_0}\right)^{0.33} \tag{8}$$

Similarly, it is possible to obtain the relation between N_e and η_d / η_0 by eliminating $\Delta\eta_m$ from Eqn. 7.

$$\frac{\eta_d}{\eta_0} = 1.68 N_e^{0.25} \tag{9}$$

Figure 13 shows the $\eta_d / \eta_0 - \Delta\eta_m / \eta_0$ relation, and Figure 14 shows the $\eta_d / \eta_0 - N_e$ relation. These figures also show the plots of Eqns. 8 and 9.

Figure 12 shows that N_e increases with a decrease in $\Delta\eta_m$. Moreover, Figure 13 indicates that η_d increases as $\Delta\eta_m$ decreases. When $\Delta\eta_m / \eta_0 = 0.1$, the energy absorption capacity is four times larger than η_0 on the lower-limit line. The energy absorption capacity per cycle decreases with an increase in the number of loading cycles. However, in Figure 14, it is observed that η_d increases with N_e.

The plots shown in black in all figures correspond to the F2 and L2 failure modes. The energy absorption capacity of specimens under cyclic loading is larger that that of other test specimens. Therefore, the plots in these figures are far from the lower-limit line, while the values of the parameters plotted in the figures tend to shift closer to the lower-limit line when the width-thickness ratio of the specimens increases.

A prerequisite for this lower-limit line is that the positive and negative amplitudes of cyclic loading are almost equal. When deformation occurs largely on either the positive or negative side, as in the case of G3BR-RE, it is noteworthy that the actual energy absorption amount is smaller than the lower-limit line.

6. CONCLUSIONS

In this study, we experimentally investigate the influence of the cyclic loading history on the energy absorption capacity of H-shaped steel beams. The following are the conclusions of this investigation:

1. It has been found that although the specimens have identical shapes, they exhibit different failure modes.
2. The energy absorption capacity (η_0) of local-buckling-type specimens under monotonic loading can be estimated using the equation proposed by Kato et al.
3. The equation for the relation between the maximum strength ratio of (α_0) and the energy absorption capacity ($_b\eta_0$) of flange-fracture-type specimens under monotonic loading has been determined.
4. It is possible to express the relation between the energy absorption capacity of specimens under cyclic loading (η_d) and monotonic loading (η_0), the mean of half-cycle energy ($\Delta\eta_m$), and the number of effective half-cycles (N_e). This relation is obtained from the equation of the lower-limit line of the energy absorption capacity.

REFERENCES

AIJ (2007), Structural response and performance for long period seismic ground motions, Architectural Institute of Japan, 5–41.

Kato, B., Akiyama, H. and Obi, Y. (1977), Deformation characteristics of H-shaped steel members influenced by local buckling**,** *Journal of Structural and Construction Engineering (Transactions of AIJ)* **257**, 49–57.